Fuel 306 (2021) 121654

Contents lists available at ScienceDirect

Fuel

journal homepage: www.elsevier.com/locate/fuel

Full Length Article

Superior performance of Cu-Ce binary oxides for toluene catalytic oxidation: Cu-Ce synergistic effect and reaction pathways

Binghong Song [a,b], Caiting Li [a,b,*], Xueyu Du [a,b], Shanhong Li [a,b], Yindi Zhang [a,b], Yue Lyu [a,b], Qihao Zhou [c]

[a] College of Environmental Science and Engineering, Hunan University, Changsha 410082, PR China
[b] Key Laboratory of Environmental Biology and Pollution Control (Hunan University), Ministry of Education, Changsha 410082, PR China
[c] Intelligent Computing and Communication (IC2) Laboratory, Key Laboratory of Universal Wireless Communications of Ministry of Education, Beijing University of Posts and Telecommunications, Beijing 100876, China

ARTICLE INFO

Keywords:
Toluene removal
Cu-Ce oxides
Oxygen vacancies
Interface lattice oxygen
Reaction mechanism

ABSTRACT

A series of Cu-Ce binary oxides were synthesized via a facile co-precipitation method for toluene catalytic oxidation. The physicochemical properties of these samples were characterized by BET, XRD, SEM, TEM, H_2-TPR, O_2-TPD, and XPS. It reveals that Cu_1Ce_3 catalyst possesses a higher specific surface area, stronger Cu-Ce synergistic effect, and better low-temperature reducibility than other samples. Moreover, Cu_1Ce_3 catalyst exhibited superior toluene oxidation activity with 99.10% toluene removal efficiency and 97.28% CO_2 selectivity at 200 °C, as well as satisfactory stability and moisture resistance. Therefore, Cu_1Ce_3 catalyst indicates a huge potential for practical applications, such as coal-fired flue gas and spray coating industry. The reaction pathways for toluene catalytic oxidation over the Cu_1Ce_3 catalyst were further illuminated by in-situ DRIFTs. In the main pathway, toluene molecules were firstly in contact with the interface lattice oxygen, then the abstraction of H atoms occurred on the methyl group, and benzyl alcohol is considered as the primary intermediate, during which the rate-determining step is the oxidation of benzyl alcohol. In the secondary pathway, a little proportion of toluene molecules were directly oxidized into benzoic acid by the chemisorbed oxygen species. In subsequent steps, all the intermediates were converted into CO_2 and H_2O. At last, it is confirmed that the toluene oxidation over Cu_1Ce_3 catalyst involves a Mars-van-Krevelen mechanism via this study.

1. Introduction

With the acceleration of industrialization and urbanization in China, air pollution has become an increasingly alarming issue around the country. Especially the hazard of volatile organic compounds (VOCs) has been extensively emphasized in the last few years. As one of the representative species of VOCs, toluene has many emission sources, such as chemical industries, petrochemical industries, sewage treatment plants, and thermal power plants [1,2]. Besides, toluene has been widely considered as a great threat to the environment and human health [3,4].

Recently, multifarious methods have been developed rapidly to eliminate the emission of toluene, catalytic oxidation has been regarded as one of the most efficient and economical technologies [5]. Furthermore, as the main products via catalytic oxidation, H_2O and CO_2 are harmless at relatively moderate conditions [6,7]. However, there are still some drawbacks such as difficulties in preparation and low catalytic efficiency. Therefore, the design of catalysts with facile preparation and superior activity is urgently required. Various catalysts are generally classified into two types based on different active components: noble metal-based catalysts and non-noble metal oxides. Although noble metal-based catalysts have shown superior performance on the toluene catalytic oxidation at a low temperature, their large-scale applications are restricted by high cost, low stability, easy-poisoned, and easy-sintered [8–10]. Thus, concentrated efforts are being made to design and synthesize catalysts based on cheap metal oxides to be substituted for the noble metals [11,12]. Most of these researches focus on the transition metal (Mn, Fe, Co, Ni, and Cu) oxides and rare earth metal (La and Ce) oxides [13,14].

Among the transition and rare earth metal oxides, copper oxides are considered as an efficient active component for the VOCs catalytic oxidation [15–17], while cerium oxides are widely used as the best promoter referred to the high oxygen storage capacity, electron release

---

* Corresponding author at: College of Environmental Science and Engineering, Hunan University, Changsha 410082, PR China.
E-mail address: ctli@hnu.edu.cn (C. Li).

https://doi.org/10.1016/j.fuel.2021.121654
Received 26 April 2021; Received in revised form 25 July 2021; Accepted 5 August 2021

properties and the facile redox cycle between Ce^{4+} and Ce^{3+} [18,19]. Lu et al. substituted part of Mn in Cu–Mn catalysts with Ce to synthesize Cu-Mn-Ce ternary oxides for toluene oxidation, and found the coexistence of Cu–Mn mixed oxides and the ceria-based solid solution resulted in a better synergetic interaction [20]. Ahmed Ismail et al. synthesized $Co_xCe_{1-x}O_{2-\delta}$ through non-ionic surfactant hydrothermal method and applied for catalytic toluene oxidation, and claimed the good activity can be mainly attributed to the strong interaction between Co and Ce oxides to form $Co_{0.2}Ce_{0.8}O_{2-\delta}$ solid solution [21]. In cerium oxides, the valence state of cerium can switch between III and IV, which makes cerium easily replaced by elements with lower oxidation states such as copper [22,23]. It leads to the formation of Cu-Ce solid solution and the production of abundant vacancies. It is believed that the synergistic effect between Cu-Ce mixed oxides by forming solid solutions is also greatly beneficial to facilitate the catalytic performance [24]. Besides, the interaction between organic molecules and active oxygen species via the filling of oxygen vacancy by gaseous oxygen is the basis of catalytic oxidation [25]. Hence, Cu-Ce composite oxides are regarded as a promising catalyst for the oxidation of toluene, and their catalytic activity is expected to be comparable with noble metal catalysts [26]. Even if this ascendant activity of Cu-Ce binary metal oxide for toluene catalytic oxidation has been widely reported in recent years, there are still some problems worth being noticed, such as low dispersion and the large gap from ignition temperature to the complete oxidation temperature of the catalytic process [27–29]. Besides, the known details about the bimetallic interaction and catalytic pathways are limited.

In the present work, a series of Cu-Ce binary oxides with different molar ratios were prepared systematically by a facile co-precipitation process. Toluene was selected as the probe pollutant for the assessment of catalytic activities. The emphases of this study are on four aspects: (I) the physicochemical properties and the details about the bimetallic interaction of the samples were characterized by BET, XRD, SEM, TEM, H_2-TPR, O_2-TPD, and XPS; (II) the effect of the molar ratio in the prepared catalysts and reaction temperatures for the toluene removal was investigated; (III) a series of tests were carried out concerning the application of the catalyst in practical occasions, not merely the influence of space velocity and gas component (O_2, NO, and H_2O), but also the evaluation of stability and CO_2 selectivity over the catalyst; (IV) the catalytic reaction pathway and the atomic-level reaction mechanism were presented by the in-situ DRIFTs technique.

2. Experimental

2.1. Sample preparation

The chemical reagents (including NaOH, $Cu(NO_3)_2$, and $Ce(NO_3)_3{\cdot}6H_2O$) were purchased from Aladdin Industrial Corporation. All the chemicals are of A.R. grade and used directly without further purification. Cu-Ce binary oxides were prepared via a facile co-precipitation method. The procedures are as follows: appropriate amounts of copper nitrate and cerium nitrate were dissolved in 100 mL deionized water. After that, 2 mol/L NaOH solution was added to the prepared solution dropwise with vigorous stirring until pH reached 11. The obtained precipitate was stirring for 4 h and then aged 2 h without any agitation at 30 °C in a constant temperature water bath. Subsequently, the precipitates were collected and washed several times with ultrapure water until the pH decreased to 7. Thereinto, it is crucial to get rid of Na^+ via the cleaning of the precipitant, the content of Na^+ must be ensured below the detection limit by inductively coupled plasma-atomic emission spectrometry (ICP-AES). Then the solid matter was dried at 50 °C in a vacuum drying chamber overnight and calcined in a muffle furnace at 500 °C for 4 h with the heating rate of 3 $°C{\cdot}min^{-1}$. Finally, the obtained Cu-Ce binary oxides were marked as Cu_1Ce_x, where x represented the molar ratio of Ce/Cu.

2.2. Characterizations and catalytic activity measurements

More details characterization and catalytic activity measurement procedures were provided in the Supplementary Information file.

2.3. Catalytic activity measurements

The experimental setup of the prepared samples for toluene catalytic oxidation is shown in Fig. S1. The catalytic activity was evaluated on a vertical fixed bed tubular quartz reactor (i.d. = 6.00 mm, length = 600 mm). The continuous flow contained 1000 ppm toluene which was generated from a bubbling bottle immersed in an ice-water bath, 21 vol % O_2, and pure N_2 as balance. And the total volume of the flow is 150 mL/min maintained by the mass flow controller for each test. 400 mg of catalysts was loaded in the reactor, corresponding to a gaseous hourly space velocity (GHSV) of 30,000 h^{-1}. By the way, the effect of GHSV on toluene removal was estimated by altering the volume of the gas flow.

The temperature window of the test is 120–300 °C monitored by a thermocouple in the reactor. The temperature was stabilized by a programmed heating device, each temperature point was maintained for 2 h to ensure the stable toluene concentration of the outlet. For instance, after the efficiency test of Cu_1Ce_3 treatment of toluene at 160 °C for 2 h, the temperature of the reaction bed was automatically raised to 180 °C at a heating rate of 3 °C/min, and the efficiency of 180 °C was obtained after treatment for 2 h.

The inlet and outlet toluene were monitored by an online gas chromatograph (GC, GC-2014C, SHIMADZU) equipped with FID. The removal efficiency of toluene ($E_{toluene}$) and the CO_2 selectivity were calculated via the following formulas:

$$E_{toluene}(\%) = \frac{\Delta(toluene)}{(toluene)_{in}} = \frac{(toluene)_{in} - (toluene)_{out}}{(toluene)_{in}} \times 100\% \tag{1}$$

where $(toluene)_{in}$ and $(toluene)_{out}$ represented the toluene concentration of inlet and outlet (ppm), respectively.

The CO_2 selectivity (C_{CO_2}):

$$C_{CO_2} = \frac{(C_{CO_2})_{out}}{7(toluene)_{in}} \times 100\% \tag{2}$$

where $(C_{CO_2})_{out}$ represented the CO_2 concentration of the outlet monitored by PGA-650 (Phymetrix, USA) (ppm).

All the tests were carried out three replicates to reproduce the results and reduce experimental error.

3. Results and discussion

3.1. Characterization of catalysts

3.1.1. N_2 adsorption–desorption

The N_2 adsorption–desorption isotherms and the curves of the pore size distribution for Cu-Ce binary oxides are shown in Fig. 1(a). All the Cu-Ce catalysts exhibited Langmuir type-IV physisorption isothermals with the H1 hysteresis loops. It confirmed that the average pore diameter of Cu-Ce binary oxides is in the mesoporous range. With the increasing of cerium contents, the hysteresis loops tended to be narrow, indicating the cerium species might contain some micropores [30]. The pore size distribution curves of Cu-Ce catalysts exhibited one single peak centered at 3.799–3.829 nm, which indicates that the distribution of mesopores is uniform. As is known, the dimension of toluene is 5.83 Å, which is far smaller than the pore diameters of the Cu-Ce catalysts. Therefore, toluene molecules could easily be adsorbed on the inner surface of the Cu-Ce binary oxides in the toluene catalytic oxidation process [31]. The specific surface area, average pore diameter, and total pore volume are listed in Table 1. The Cu_1Ce_3 catalyst reaches the maximum value of specific surface area (76.871 m^2/g) and pore volume (0.101 cm^3/g), which could provide abundant adsorption sites.

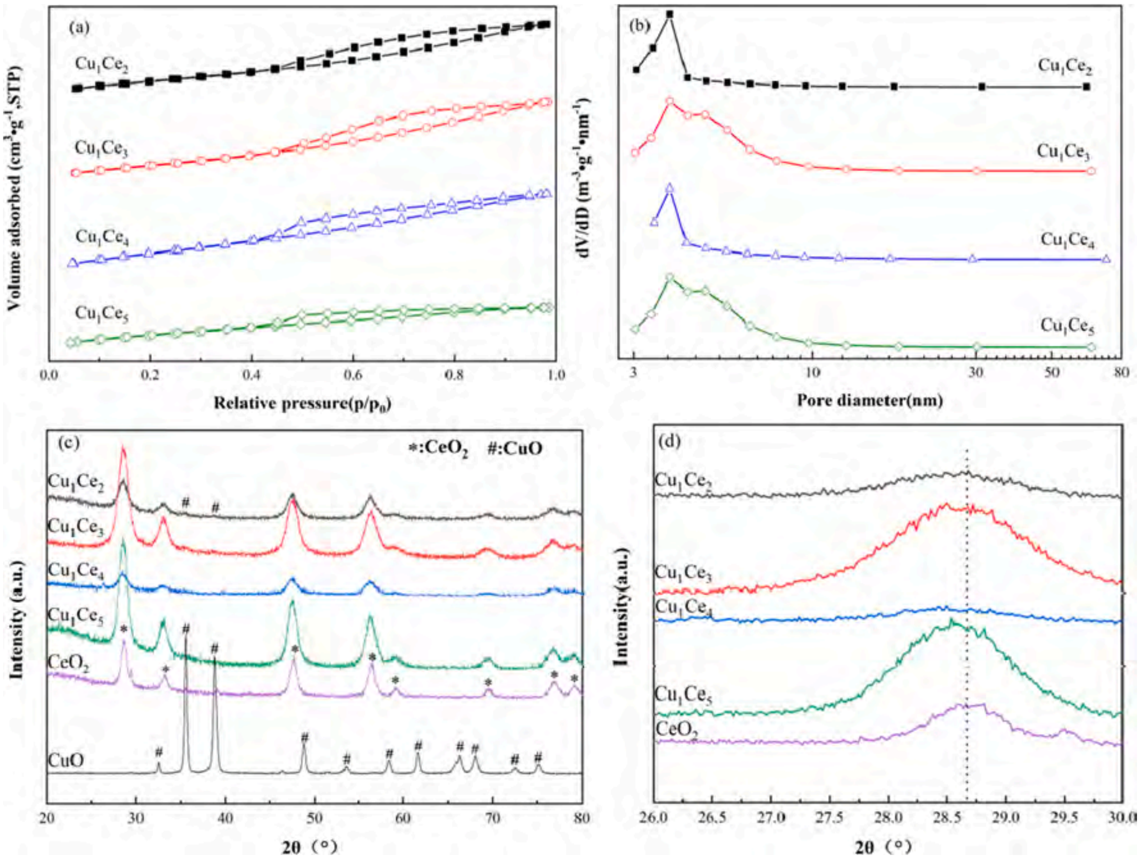

Fig. 1. (a) Nitrogen adsorption–desorption isotherms and (b) pore diameter distribution of the catalysts; (c) XRD patterns of the samples; (d) The magnified XRD patterns.

Table 1

Specific surface area, pore parameters, H_2 consumption, O_2 desorption and crystal size of the catalysts.

Sample	Crystal size (nm)	Specific surface area (m^2/g)	Pore diameter (nm)	Pore volume (cm^3/g)	H_2 consumption (mmol/g)	O_2 desorption (mmol/g)
CuO	20.11	–	–	–	–	1.294
CeO_2	11.79	–	–	–	–	–
Cu_1Ce_2	6.17	70.193	3.799	0.091	1.061	2.972
Cu_1Ce_3	5.61	76.871	3.829	0.101	0.782	2.931
Cu_1Ce_4	7.16	68.079	3.828	0.085	0.707	2.633
Cu_1Ce_5	7.45	49.123	3.828	0.051	0.368	2.089

3.1.2. XRd

The XRD patterns displayed in Fig. 1(c) are indexed to match the standard patterns (JCPDS 45-0937 and JCPDS 34-0394). The peaks of CeO_2 in the Cu_1Ce_3 catalyst are more pronounced than other samples, indicating Cu_1Ce_3 catalyst possesses the relatively high crystallinity CeO_2. From previous studies [32], high crystallinity CeO_2 in the Cu-Ce binary oxides promotes the saturated capacity for incorporated CuO. Furthermore, once the content of copper species exceeds the capacity limitation, copper clusters might tend to aggregate. Thus, two small addition diffraction peaks related to CuO are observed at 35.6° and 38.8° in the Cu_1Ce_2 catalyst. As the content of copper species decreased, the peaks assigned to CuO appeared to vanish. It suggests that small copper species could be well dispersed on the ceria surface or incorporated into the ceria matrix. As is illustrated in Fig. 1(d), peaks at 28.7° were further magnified. Compared to the pure CeO_2, a slight shift to left of CeO_2 peak could be observed for all the Cu-Ce catalysts, from which we could learn that copper species incorporated into the lattice of CeO_2 via the co-precipitation process. [33]. The crystal sizes of the samples calculated by the Debye-Scherrer equation are summarized in Table 1. The crystal sizes of Cu-Ce binary oxides (5.61–7.45 nm) become smaller compared with the pure CeO_2 (11.79 nm). It can be inferred that the partial Ce^{4+} was taken place by Cu^{2+}, leading to a constriction of the Ce-O bond [34,35]. Among all the Cu-Ce binary oxides, Cu_1Ce_3 exhibited the smallest crystal size. It implied that more copper species were introduced into the CeO_2 lattices, resulting in the formation of abundant structural defects on the Cu_1Ce_3 catalyst.

3.1.3. Morphologic and structural characterizations

The morphology of pure CuO, CeO_2, and Cu-Ce binary oxides was investigated by FE-SEM in Fig. 2. Pure CuO exhibited an aggregated polyhedral structure, while pure CeO_2 showed a lamellar structure with a small number of dispersed particles on the surface. By comparison, the Cu-Ce binary oxides exhibited grape-shaped nanoparticles, indicating the copper species were dispersed on the surface of ceria support. However, significant agglomeration was observed on the Cu_1Ce_2 and Cu_1Ce_5 catalysts. Considering the results from XRD, the agglomerates on the Cu_1Ce_2 catalyst could be identified as bulk CuO, which suggests that the saturated capacity for CuO in ceria support had been exceeded. As for the Cu_1Ce_5 catalyst, it could be inferred that the CeO_2 particles started to appear and mixed with the grape-shaped nanoparticles

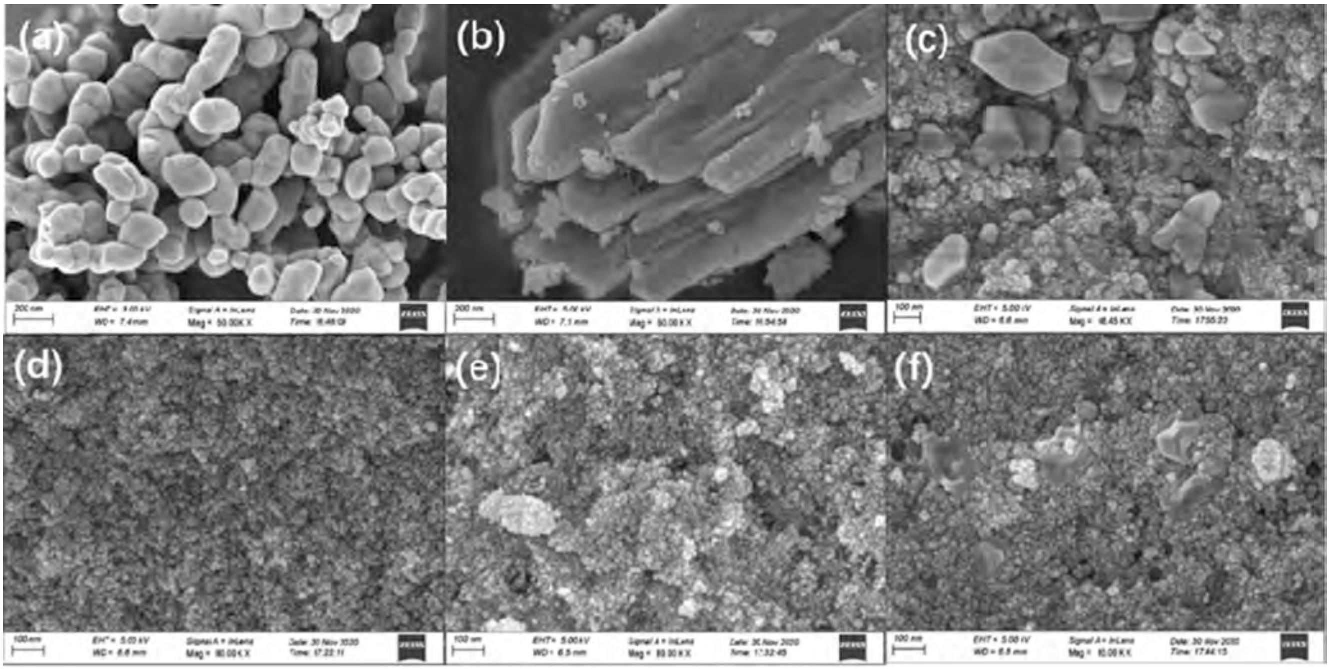

Fig. 2. FE-SEM images of (a) CuO, (b) CeO_2, (c) Cu_1Ce_2, (d) Cu_1Ce_3, (e) Cu_1Ce_4, (f) Cu_1Ce_5. The morphology, as well as the details of the bimetallic interaction of Cu-Ce.

according to the high content of cerium species. Besides, among all the Cu-Ce binary oxides, nanoparticles on Cu_1Ce_3 are dispersed most uniformly, implying a strong Cu-Ce synergistic effect [36].

The morphology, as well as the details of the bimetallic interaction of Cu-Ce binary oxides, was investigated by TEM. As is shown in Fig. 3, Cu_1Ce_2 (Fig. 3(a)) and Cu_1Ce_5 (Fig. 3(d)) catalysts were seriously agglomerated, the particles of these catalysts have clumped into bulks, while the Cu_1Ce_3 catalyst exhibited the best dispersion with the particle size of 5–7 nm, which is consistent with the observation of FE-SEM. The highest surface area of Cu_1Ce_3, as demonstrated in Table 1, should be responsible for it. The High-Resolution TEM image of Cu_1Ce_3 catalyst is shown in Fig. 3(e), the spacings of lattice fringes were measured as 0.269 nm and 0.312 nm, which were indexed to match the (1 1 0) plane of CuO and the (1 1 1) plane of CeO_2, respectively [37]. Interestingly, the distortion of CeO_2 lattice fringes between the nanoparticles could be easily distinguished in Cu_1Ce_3 catalysts, which implies the Cu-Ce amorphous solid solution was formed at the interface between CuO and CeO_2 [38]. According to Fig. S2, it could be learned that this distortion is present in all the Cu-Ce binary oxide samples. Combined with the slight shift of CeO_2 characteristic peak at 28.7° in XRD (Fig. 1 (d)), it could be concluded that the incorporated Cu ions into CeO_2 are beneficial for the formation of the amorphous solid solution, finally

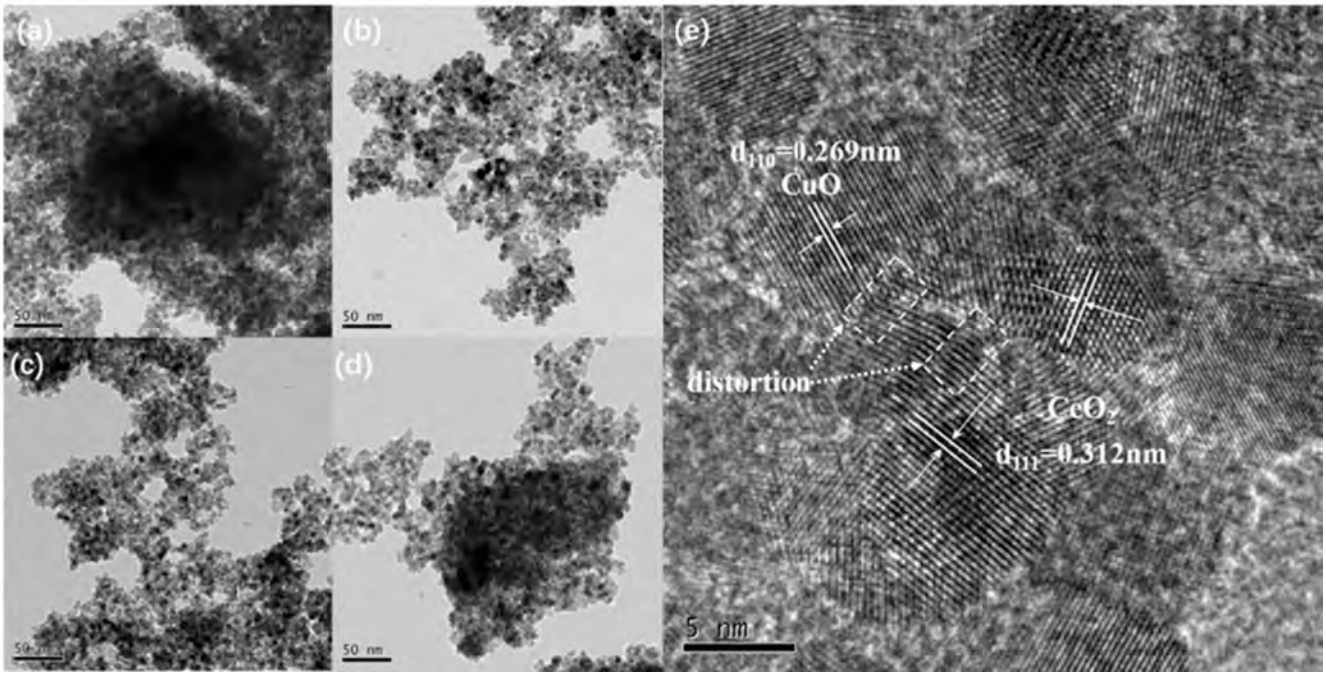

Fig. 3. TEM images of (a) Cu_1Ce_2, (b) Cu_1Ce_3, (c) Cu_1Ce_4, (d) Cu_1Ce_5 and the HRTEM image of (e) Cu_1Ce_3.

leads to the structural defects. The oxygen vacancies could be generated via these structural defects, resulting in the formation of O_v-Cu^{2+}-O-Ce^{4+} connection [36]. Accordingly, the mobility of oxygen species had been enhanced, which further improve the catalytic activity over Cu_1Ce_3 catalyst.

3.1.4. Raman analysis

Raman spectra of all the samples are shown in Fig. 4. In pure CeO_2, the peak located at 463.88 cm^{-1} could be attributed to the symmetric breathing mode of oxygen atoms around cerium ions [39]. It is obviously that the peaks become weak and broaden in the serial Cu-Ce binary oxides. This phenomenon might be attributing to the changes in the lattice parameter with crystal size and phonon confinement [40–42]. Besides, a down-shifts could be also observed in the spectra of Cu-Ce binary oxides. The down-shifts might be also related with oxygen vacancies [43], which are originated from structural defects due to partially incorporation of copper into CeO_2 lattice, in agreement with the decrease of crystal size calculated by the Debye-Scherrer equation. Moreover, the amount of oxygen vacancy over various catalysts (see Fig. 4(b)) was further calculated by Gaussian deconvolution the region around 598 cm^{-1} [44]. It can be observed that the Cu_1Ce_3 catalyst possesses highest oxygen vacancy concentration.

3.1.5. XPs

The chemical states and the compositions on the surface of the obtained catalysts were elucidated by XPS analysis. Fig. 5 demonstrated the fitting results of the O1s, Cu 2p, and Ce 3d. Furthermore, the datum of XPS was summarized in Table S1. The O 1s XPS spectra are plotted in Fig. 5(a), which could be fitted into three peaks. The O 1s signals with binding energy from 533.47 to 535.08 eV, 530.34 to 531.38 eV and 528.38 to 529.27 eV correspond to surface hydroxyl oxygen (denoted as O_α), chemisorbed O_2 (denoted as O_β) and lattice oxygen (denoted as O_γ) on the catalysts, respectively [45–48]. The O_β contents of the Cu-Ce binary oxides calculated by $O_\beta/(O_\alpha + O_\beta + O_\gamma)$ are summarized in Table S1. The O_β ratio of Cu_1Ce_3 catalyst is much higher than those of other samples. According to previous reports [49,50], the chemisorbed O_2 (O_β) could not only boost the adsorption of oxygen from the gas phase through its high mobility but also facilitate catalytic oxidation by connecting metal atoms on the surface with active oxygen species via a weak bonding interaction [51]. The O_β ratio of the Cu_1Ce_3 catalyst is much higher than those of other samples. Notably, this ratio sharply decreased from 69.59% to 19.29% after the reaction, implied that the O_β was partially involved in the oxidation process.

In high-resolution of Cu 2p spectra displayed in Fig. 5(b), the Cu $2p_{3/2}$ binding energy of 931–938 eV, the Cu $2p_{1/2}$ of 952–958 eV, and satellite peaks are observed for a series of Cu-Ce binary oxides. It is well-known that the higher Cu $2p_{3/2}$ and Cu $2p_{1/2}$ binding energy is related to the Cu^{2+} species, the lower Cu $2p_{3/2}$ and Cu $2p_{1/2}$ binding energy are attributed to the reduced copper species [52,53]. The complex spectra of Ce 3d are displayed in Fig. 5(c). The two sets of spin-orbital were denoted as u and v referring to the Ce $3d_{3/2}$ and Ce $3d_{5/2}$. The Ce^{3+} relative content can be calculated via the formula: $Ce^{3+}/(Ce^{3+}+Ce^{4+})$, where $Ce^{3+} = (u' + u_0 + v' + v_0)$ and $Ce^{4+} = (u + u'' + u''' + v + v'' + v''' u + u' + u''' + v + v'' + v''')$. Based on the previous study [54], Ce^{3+} is related to the formation of oxygen vacancies and the activation of surface oxygen species, which could improve catalytic activity of Cu-Ce binary oxides in the toluene catalytic oxidation. Besides, the co-existence of Ce^{3+} and incorporated Cu^{2+} could reduce the redox potentials and facilitate the formation of Cu-Ce solid solution [55]. Therefore, it can be deduced that the oxygen vacancies and Cu-Ce interaction are present in all the Cu-Ce binary oxides. The O_v-Cu^{2+}-O-Ce^{4+} connection could be formed via this Cu-Ce interaction as illustrated in HR-TEM (Fig. 3(e)), providing a link for O transferred between Cu and Ce. It's worth noting that both the contents of Cu^{2+} and Ce^{3+} decreased after the reaction over Cu_1Ce_3 catalyst. As is known, surface defect and oxygen vacancies could be introduced in the structure via Cu ions incorporated into the lattice of ceria which can be summarized by the equilibrium $Ce^{3+} + Cu^{2+} \Leftrightarrow Ce^{4+} + Cu^{+}$. It reveals that Cu^{2+} and Ce^{3+} were partially involved in the toluene catalytic oxidation process. Compared to other samples, Cu_1Ce_3 catalysts exhibit higher Ce^{3+} and Cu^{2+} content, which might promote the activity for toluene catalytic oxidation.

3.1.6. H_2-TPr

The samples' reducibility was characterized by H_2-TPR. Fig. 6(d) illustrated the H_2-TPR profiles of Cu_1Ce_2, Cu_1Ce_3, Cu_1Ce_4, and Cu_1Ce_5. Besides, the H_2 consumption of the serial Cu-Ce oxides was calculated and listed in Table 1. The H_2 consumption gradually decreases with an increase of cerium contents, and the corresponding values range from 1.061 to 0.368 mmol/g. As shown in the XRD results, most Cu^{2+} ions exist in the form of small clusters or bulk CuO, which can be wrapped by CeO_2 during the reduction–oxidation processes. Due to the kinetic diffusion, the dispersed CuO and CeO_2 are difficult to reduce. Additionally, some Cu^{2+} in Cu-Ce solid solutions are not completely reduced. Thus, it is reasonable that the H_2 consumption decline when the contents of cerium species increase. A broad reduction peak is seen at 100–250 °C, which can be divided into three parts (α, β, γ) by peak fitting. The α reduction peak is ascribed to the dispersed copper species. The β reduction peak corresponds to the Cu ions incorporated into the frame of CeO_2. The γ reduction peak detected at a higher temperature is ascribed to the bulk or crystalline copper species which interacted weakly with CeO_2 [56]. Bulk or crystalline CuO has little contribution to

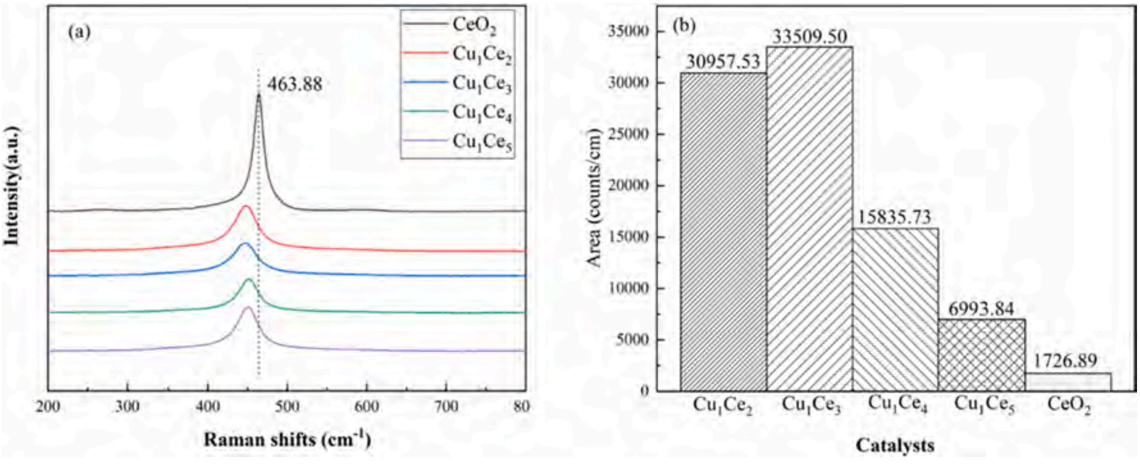

Fig. 4. (a) Raman spectra of Cu_1Ce_2, Cu_1Ce_3, Cu_1Ce_4, Cu_1Ce_5, and CeO_2; (b) integrated peak areas at 598 cm^{-1} for various catalysts.

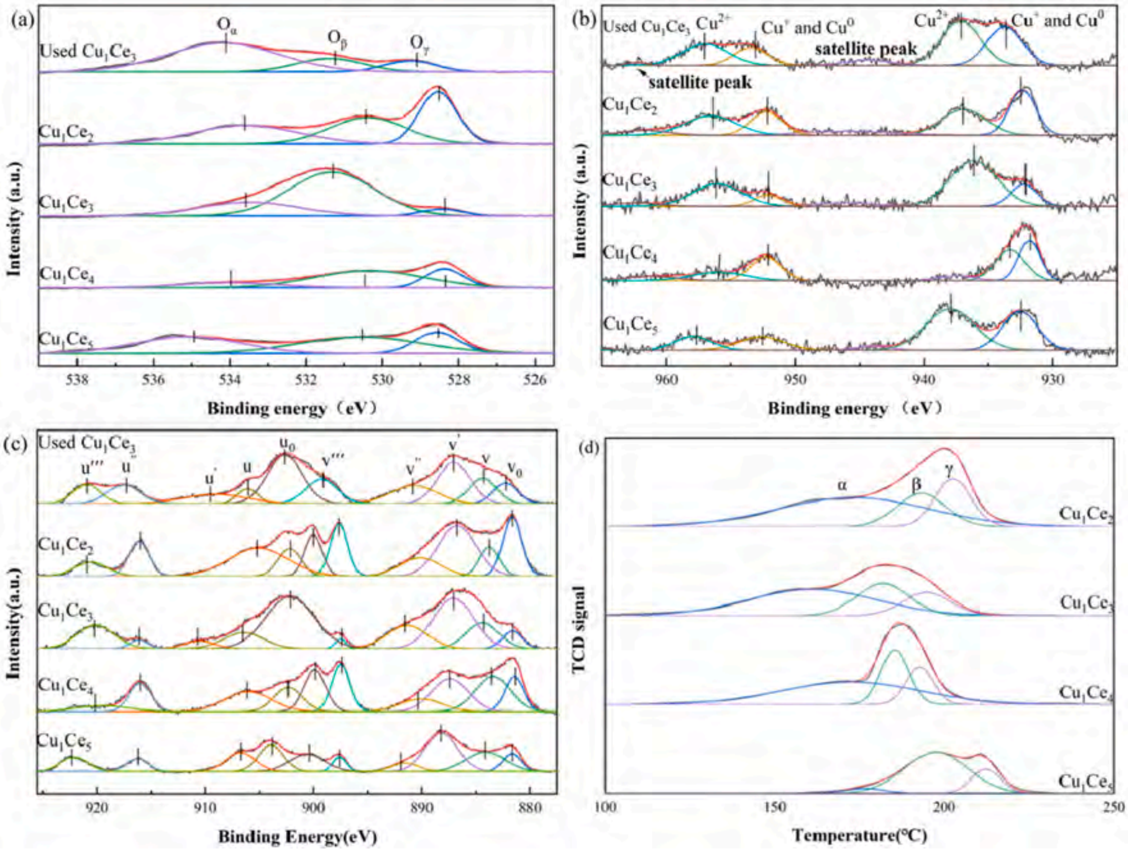

Fig. 5. XPS spectra of (a) O 1s, (b) Cu 2p and (c) Ce 3d; (d) H_2-TPR profiles of Cu-Ce binary oxide catalysts.

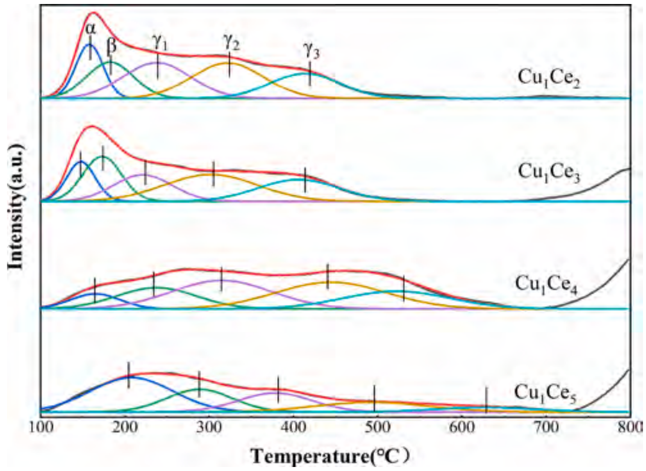

Fig. 6. O_2-TPD profiles of Cu-Ce binary oxide catalysts.

catalytic performance since it could only be reduced at a relatively high temperature. According to previous research [37], pure CuO and CeO_2 samples both indicated their reduction peak at 375 °C and 550 °C, respectively. However, the reduction peaks of all the Cu-Ce binary oxide samples here are at the temperature range of 100–250 °C, which is well below 375 °C. It could be speculated that the Cu-Ce synergistic effect promotes the reduction of the copper species. Consequently, the reduction peaks of Cu-Ce binary oxides shifted to a lower temperature. The position temperature of peak α and β ranks as $Cu_1Ce_3 < Cu_1Ce_2 < Cu_1Ce_4 < Cu_1Ce_5$. Compared to other samples, the reduction peaks of Cu_1Ce_3 catalyst were at the lowest temperature side, suggesting the reducibility was enhanced via forming Cu-Ce solid solution. The O_v-Cu^{2+}-O^{2-}-Ce^{4+} connection was built as a bridge that could facilitate O transfer between copper and cerium species by reducing the redox potential of copper species. It is believed better interaction in the Cu-Ce binary oxides promotes reducibility of copper species and improves the redox cycle in toluene oxidations [36,57]. Therefore, Cu_1Ce_3 is considered the most interesting sample.

3.1.7. O_2-TPd

The reactivity of the oxygen species was measured by O_2 Temperature programmed desorption tests (O_2-TPD) and the O_2 desorption was listed in Table 1. The O_2 desorption of Cu-Ce binary oxides was higher than that of CuO, implied a strong Cu-Ce synergistic effect. In addition, the O_2 desorption of Cu-Ce binary oxides decline when the contents of cerium species increase. Combined the profile shown in Fig. S3, CeO_2 made little contribution for O_2 desorption below 700℃, it could be inferred that copper oxides were the active component for the toluene catalytic oxidation, while cerium oxides played a role as the promoter. The O_2-TPD curves of all the Cu-Ce binary oxides are made up of five peaks below 800 °C after fitting, which was consisted with physically absorbed oxygen (peak α), chemisorbed oxygen (peak β), and lattice oxygen of CuO (peak γ). The peaks of γ_1, γ_2, and γ_3 could be ascribed to the well dispersed CuO, copper incorporated with cerium species, and bulk CuO referred to the result of H_2-TPR. With the increase of cerium content, the peaks above 700 °C, relevant to the reduction of CeO_2 lattice oxygen, were detected in the samples of Cu_1Ce_3, Cu_1Ce_4, and Cu_1Ce_5 catalysts [54]. As is displayed in Fig. 6, the Cu_1Ce_3 catalyst possesses the highest peak area of chemisorbed oxygen species, further testifying its maximum amount of O_β as identified by XPS. Meanwhile, the peaks γ of Cu_1Ce_3 shift to a lower temperature, indicating that the oxygen mobility was improved. These results are in agreement with the XPS analysis. Combined with the XPS results, a large amount of surface Ce^{3+} and incorporated Cu^{2+} are concentrated on the Cu_1Ce_3 catalyst, which is related to more oxygen-supplying centers. Moreover, the O_V-Cu^{2+}-O-Ce^{4+} connection can be formed via the Cu-Ce synergistic effect in the Cu_1Ce_3 oxides. Thus, it is confirmed that the oxygen transformation between Cu and Ce could be facilitated.

3.2. *Catalytic performance*

3.2.1. *The effect of Ce/Cu molar ratio*

A blank test without catalyst was performed to exclude interaction between toluene and the reactor at first. There was no significant removal of toluene detected below 300 °C. The catalytic conversion of toluene over CuO, CeO_2, and four Cu-Ce binary oxides versus reaction temperature was displayed in Fig. 7. Pure CeO_2 exhibited the worst catalytic performance, while pure CuO reached a toluene conversion of over 90% at 280 °C. According to the result of H_2-TPR and O_2-TPD, the reduction peak and desorption peak of the lattice oxygen in CeO_2 was detected over 700 °C, it can be speculated that the lattice oxygen in CeO_2 has little contribution to the catalytic oxidation of toluene at low temperature. Therefore, CeO_2 might be regarded as support while copper species could be considered as the active components in the toluene catalytic oxidation. Beyond that, Cu-Ce binary oxides exhibited better toluene catalyst activity than the single metal oxides, indicating the strong Cu-Ce synergistic effect was beneficial to toluene catalytic oxidation. Thereinto, the Cu_1Ce_3 catalyst showed the best toluene removal efficiency of Cu-Ce binary oxides, which reached 96.91% at 180 °C and 99.10% at 200 °C, respectively. Based on the result of this test, the Cu_1Ce_3 catalyst was used for further study.

3.2.2. *The effect of space velocity*

In practical industrial applications, space velocity is considered a crucial parameter in catalytic oxidation [58]. Hence, the effect of space velocity on toluene catalytic oxidation over Cu_1Ce_3 catalyst was tested. As is shown in Fig. 8, with the increase of GHSV, the activity of the Cu_1Ce_3 catalyst tended to decrease. The trend is in line with expectations since it is believed that toluene retention time is positively correlated with catalyst activity. Even with a GHSV at 180000 h^{-1}, the Cu_1Ce_3 catalyst could still achieve over 90% toluene conversion rate at 280 °C. It suggests that the Cu_1Ce_3 catalyst could keep a considerable catalytic activity under high GHSV conditions in actual application.

3.2.3. *The effect of gas components*

Effects of gas components (O_2, NO, and H_2O) on toluene catalytic oxidation over Cu_1Ce_3 catalyst at 210 °C are displayed in Fig. 9.

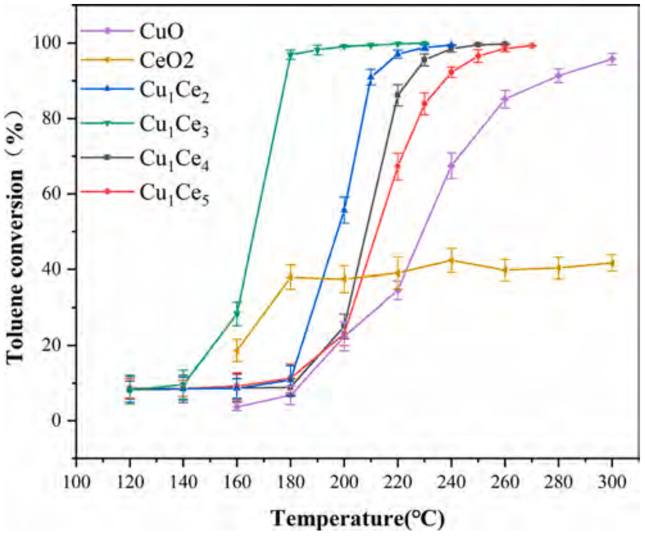

Fig. 7. Toluene conversion over Ce/Cu molar ratio (Reaction conditions: 120–300 °C, 1000 ppm toluene, 21 vol% O_2, N_2 as balance, GHSV = 30,000 h^{-1}).

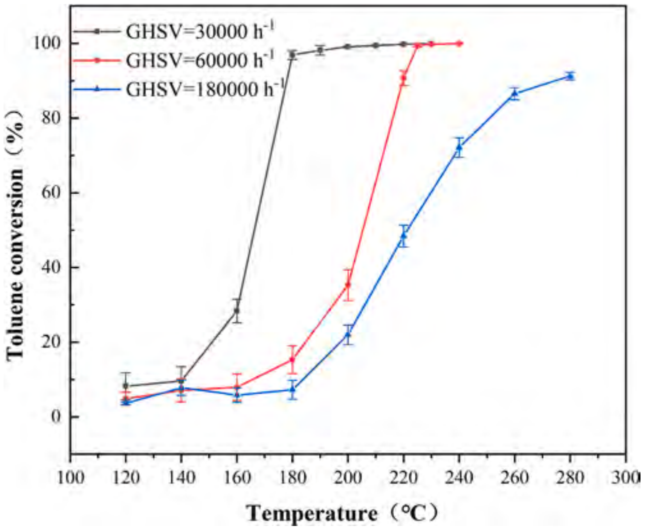

Fig. 8. The effect of GHSV (Reaction conditions: 1000 ppm toluene, 21 vol% O_2, N_2 as balance, GHSV = 30,000–180,000 h^{-1}).

O_2 is considered as a momentous gas component, the concentration of O_2 in industrial exhaust gases may vary from field to field. From Fig. 9, the Cu_1Ce_3 catalyst exhibited a relatively low activity in the absence of oxygen, and decreased over time, implying the consumption of surface chemisorbed O_2 turned into an irreversible step without the replenishment of gaseous oxygen [47]. After 6 vol% O_2 was added into the stream, the conversion of toluene boosted from 9.55% to 91.36% within 30 min, then stabilized at 96% to 97%. When 21 vol% O_2 was added, the toluene conversion was promoted again over 99%. It reveals that O_2 from gas phase played a key role in toluene catalytic oxidation. The surface adsorbed oxygen on catalyst could be replenished from gas-phase O_2, which leads to the regeneration of lattice oxygen in the catalyst. Besides, it could be seen that the Cu_1Ce_3 catalyst achieved over 96% toluene conversion at 6 vol% O_2, indicating Cu_1Ce_3 catalyst may be an option worth further considering for low oxygen content conditions, like coal flue gas.

Several researchers considered volatile organic compounds (VOCs) as one of major precursors for ground-level ozone formation after a

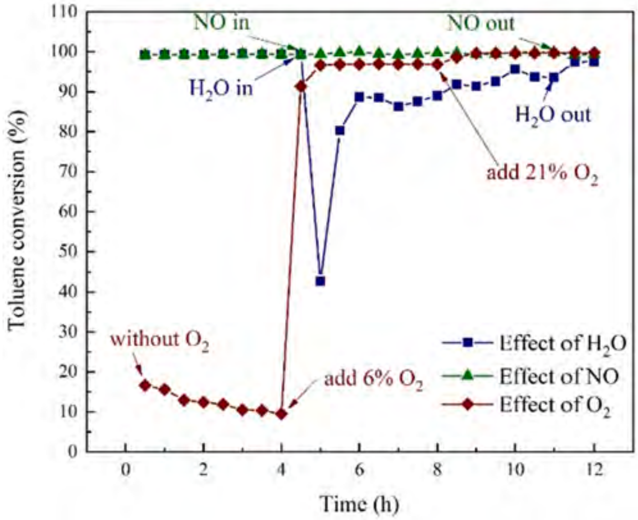

Fig. 9. The effect of gas components (Reaction conditions: 210 °C, 1000 ppm toluene, 0–21 vol% O_2, 0–400 ppm NO, 0–10 vol% H_2O, N_2 as balance, GHSV = 30,000 h^{-1}).

series of complex atmospheric chemical reactions together with NO_x [46]. It was reported that NO could occupy the active sites and consume the active oxygen species, resulting in the deactivation of the catalyst [59,60]. However, there was no significant change and even a slight improvement in the toluene conversion after 400 ppm NO was introduced. It could be ascribed to the replenishment of active oxygen species by O_2 from the gas phase, but more importantly, the NO_2 generated under aerobic conditions could facilitate the activation for the subsequent toluene [61,62]. Presumably, the stronger oxidizing property of NO_2 led to the improvement of toluene conversion.

The effect of 10 vol% H_2O on toluene conversion over Cu_1Ce_3 catalyst was evaluated to explore further practical applications. When 10 vol % H_2O was introduced into the feed at 4 h, the toluene conversion fell from 99.29% to 42.63% at first within 30 min, then climbed rapidly and finally stabilized at over 90% during 8–11 h. Once 10 vol% H_2O was removed, the toluene conversion increased again and was nearly recovered to the original level. It suggests that the Cu_1Ce_3 catalyst exhibited good water resistance and the slight deactivation caused by 10 vol% H_2O is reversible. On the one hand, the competitive adsorption of toluene and water vapor on the active sites over Cu_1Ce_3 catalyst inhibited the catalytic performance, on the other hand, water vapor may promote the catalytic oxidation of toluene as a hydrolysis agent and hydrogen-supplying agent [63]. Thus, it could be concluded that the addition of 10 vol% H_2O may have a significant effect on the intermediates but a slight effect on the toluene conversion.

3.2.4. The durability and CO_2 selectivity

To measure the durability and CO_2 selectivity of the Cu_1Ce_3 catalyst, the removal of toluene and the yield of the CO_2 were monitored at the temperature window of 120 °C to 230 °C. Then, the oxidation process was conducted for 120 h at 210 °C. As is presented in Fig. 10(a), the curve of toluene removal and CO_2 yield both increased with the temperature. At 200 °C, it was detected that the removal of 1040.46 ppm toluene and the yield of 7085.00 ppm CO_2 at the same time, which implies CO_2 selectivity reached 97.279%. Moreover, the CO_2 selectivity kept increasing with temperature and stabilized at above 98% over 210 °C. Notably, at the temperature of 180 °C, although the toluene removal efficiency reached 96.91%, the CO_2 selectivity was only 79.70%, it could be deduced that some intermediates could be emitted into the air at 180 °C. It is believed that the interaction between organic molecules and active oxygen species at oxygen vacancies is the basis of catalytic oxidation [25]. Presumably, toluene adsorbed on the oxygen vacancies could be oxidized into some intermediates at a low temperature and further oxidized into CO_2 and H_2O at a higher temperature. Hence, the optimum temperature for the toluene catalytic oxidation depends not only on the removal efficiency but also on the CO_2 selectivity.

As is shown in Fig. 10(b), the conversion efficiency curve of toluene over Cu_1Ce_3 catalyst kept stable above 99% at 210 °C with little fluctuation. Meanwhile, the curve of CO_2 selectivity is slightly lower than it, remained above 98%, which implies a very small quantity of intermediates was generated in toluene catalytic oxidation within 120 h. This test confirmed a superior stability and CO_2 selectivity of the Cu_1Ce_3 catalyst, and it shows that Cu_1Ce_3 binary oxide might be regarded as a choice of an environment-friendly catalyst in industrial applications.

3.3. In-situ DRIFTs

To track the transient species during the toluene catalytic oxidation process clearly, the in-situ DRIFTs were recorded to monitor the intermediates over the Cu_1Ce_3 catalyst. The test procedure was described in supporting information.

Fig. 11(a) shows the infrared signal from toluene and a series of intermediates over the Cu_1Ce_3 catalyst at 210 °C with time. The band at 1222 cm^{-1} can be ascribed to the symmetric stretching C–C band, the bands at 1447 cm^{-1} and 1597 cm^{-1} are assigned to the symmetric stretching $C = C$ band of the aromatic ring [12,64]. Moreover, the band at 3082 cm^{-1} is corresponded to C–H asymmetric or symmetric stretching vibration of methyl [65]. These bands were observed after 5 min contacted with toluene, which implies the existence of adsorbed toluene on the Cu_1Ce_3 catalyst. A strong band at 1142 cm^{-1} is ascribed to the C–O stretching vibration of alkoxide species [66]. Meanwhile, the band at 2874 cm^{-1} is assigned to C–H asymmetric or symmetric stretching vibration of methylene [67]. Presumably, the primary reaction step of toluene catalytic oxidation might be hydrogen abstraction. It suggests that the oxidation process began at the side chain of the methyl group since the weakest band in the toluene molecule is precisely the C–H band of this group. Therefore, the hydrogen atom was abstracted easily by •OH and the benzyl alcohol would be formed. The bands at 1409 cm^{-1}, 1812 cm^{-1}, 1920 cm^{-1} and 1963 cm^{-1} could be observed at the time of 20 min. The band at 1409 cm^{-1} is related to the bending vibration of O–H group, which is assigned to benzoate [64]. The bands at 1812 cm^{-1}, 1920 cm^{-1} and 1963 cm^{-1} could be assigned to maleic anhydride species [68]. It could be deduced that the benzyl alcohol was further oxidized into benzoate and maleic anhydride. Notably, all the processes above were carried out without the presence of gaseous oxygen, since the adsorbed oxygen was removed via pretreatment, which implies the consumption of the lattice oxygen species. At the time of 30 min, 21 vol% O_2 was introduced into the IR cell, it could be observed that almost all the bands started to decrease at 35 min, except the band at 1409 cm^{-1}. This band gradually increased at first, then vanished after 50 min. It implies the oxygen vacancies were replenished by the gaseous oxygen and the oxidation of benzyl alcohol was accelerated, resulting in the accumulation of benzoate. At the time of 60 min, all the peaks are

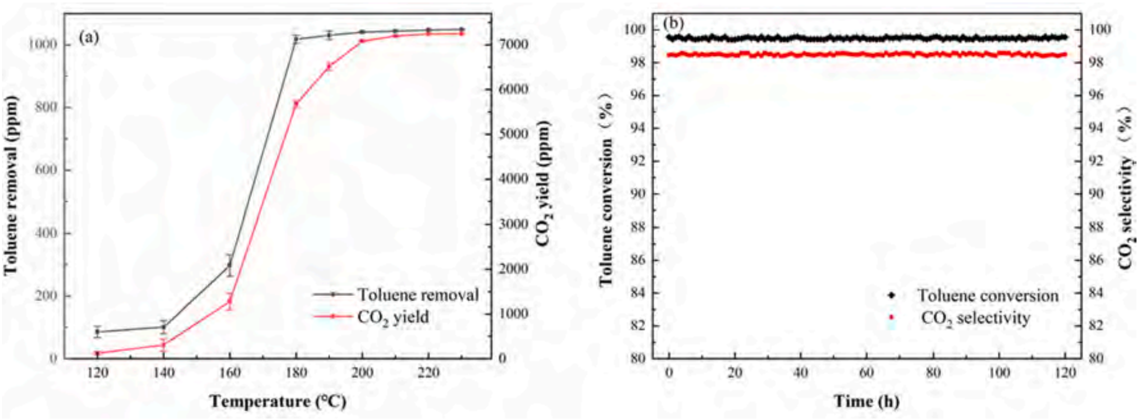

Fig. 10. (a) CO_2 selectivity (Reaction conditions: 120–230 °C, 1000 ppm toluene, 21 vol% O_2, N_2 as balance, GHSV = 30,000 h^{-1}); (b) durability (Reaction conditions: 210 °C, 1000 ppm toluene, 21 vol% O_2, N_2 as balance, GHSV = 30,000 h^{-1}).

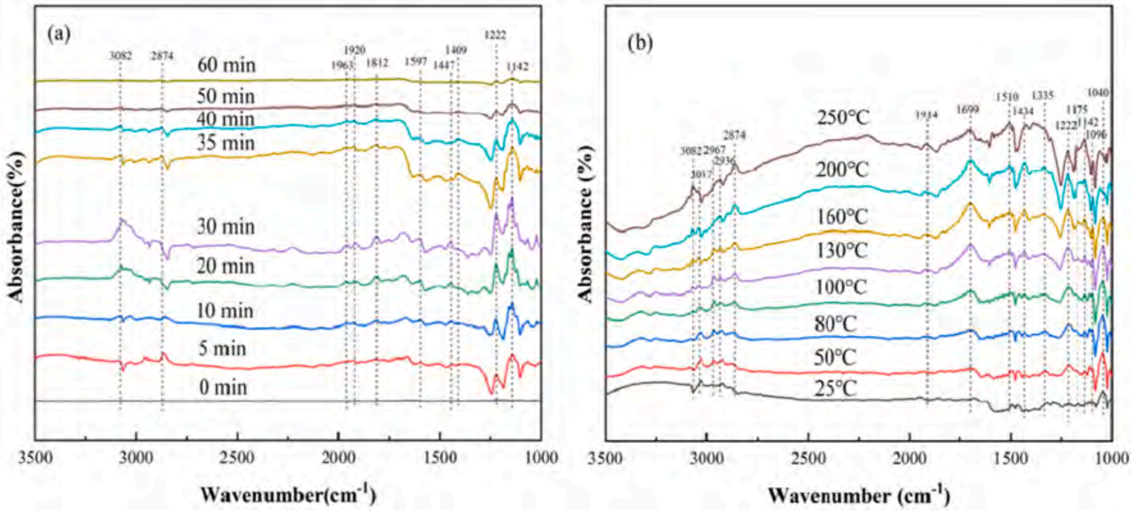

Fig. 11. In-situ DRIFTs analysis on Cu_1Ce_3 catalyst under different conditions.

nearly disappeared, indicating that the toluene is completely oxidized to CO_2 and H_2O.

Fig. 11(b) shows the process of toluene catalytic oxidation, the spectra at elevated temperatures were recorded. The band at 1040 cm^{-1} is assigned to the in-plane toluene C–H bending [69]. The bands at 2967 cm^{-1} and 3037 cm^{-1} are ascribed to the C–H stretching vibration of methyl group and aromatic rings, respectively. Combined with the bands mentioned earlier at 1222 cm^{-1} and 3082 cm^{-1}, it can be inferred the toluene was absorbed on the Cu_1Ce_3 catalyst. The bands observed at 1096 cm^{-1}, 1142 cm^{-1} and 1175 cm^{-1} are assignable to benzyl alcohol [66]. Meanwhile, the bands at 1335 cm^{-1}, 1510 cm^{-1} and 1699 cm^{-1} are assigned to benzoate. The bands assigned to benzyl alcohol tended to be stronger with the temperature increasing. A possible reason is the oxidation of toluene might be accelerated as the temperature increased, resulting in the accumulation of benzyl alcohol. Thus, the oxidation of benzyl alcohol could be considered as the rate-determining step. Besides, the bands at 2861 cm^{-1} and 1936 cm^{-1} are assigned to methylene. According to the hydrogen abstraction mentioned above, it could be inferred that benzyl alcohol is the primary intermediate. The bands at 1335 cm^{-1} and 1699 cm^{-1} become weaker above 200 °C while the band at 1510 cm^{-1} still appears to be stronger. It suggests the benzoate related to 1335 cm^{-1} and 1699 cm^{-1} could only be originated from the primary intermediate and was easily consumed as the temperature increased; while the benzoate assigned to 1510 cm^{-1} could be generated directly by the oxidized of toluene with the presence of gaseous oxygen [70]. The bands at 1434 cm^{-1} and 1914 cm^{-1} are assigned to maleic anhydride, indicating that the aromatic ring was broken. The intermediates without the aromatic ring are easily further oxidized into CO_2 and H_2O [67].

Thus, the reaction pathway for toluene catalytic oxidation over Cu_1Ce_3 catalyst could be concluded. The hydrogen abstraction is the primary step, and the main reaction pathway is presented as follows: toluene → benzyl alcohol → benzoic acid → maleic anhydride → CO_2 and H_2O.

3.4. Possible reaction mechanism

It is well accepted that the organic molecules catalytic oxidation over the transition metal oxides is primarily carried out with the participation of lattice oxygen [28,71,72]. To further illuminate the reaction pathways over Cu_1Ce_3 catalyst, a possible reaction mechanism on Cu-Ce solid solution was displayed in Fig. 12. In the beginning, a majority of toluene molecules could be connected with the oxygen species at oxygen vacancies, catalytic oxidation process occurred via the abstraction of H atoms from the weakest side chain of methyl. Subsequently, the surface hydroxide ions were formed, resulting in the generation of benzyl alcohol. With a simultaneous replenishment process via the redox cycle $Ce^{4+} + Cu^{+} \Leftrightarrow Ce^{3+} + Cu^{2+}$, the consumed lattice oxygen could be regenerated by gas-phase oxygen. After that, the generated benzyl alcohol was successively transformed into benzoic acid. Meanwhile, a little portion of toluene adsorbed on the Cu_1Ce_3 catalyst could be directly

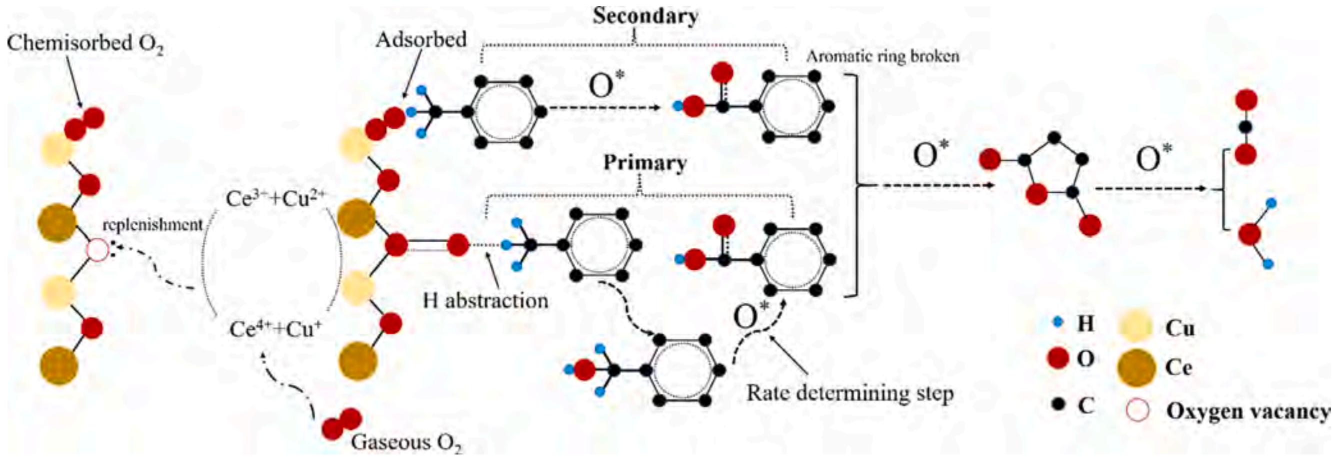

Fig. 12. The proposed mechanism of toluene catalytic oxidation over Cu_1Ce_3 catalyst.

oxidized into benzoate species by these replenished surface oxygen species [25]. Then, maleic anhydride was generated as the aromatic rings were broken. Finally, all the intermediates would be oxidized into CO_2 and H_2O. In MvK model, the oxidation of VOCs takes place in two steps. The first step is the reaction of adsorbed oxygen on the catalyst surface and molecule in the gas phase, which is followed by the generation of a product on the surface, and the desorption of that product from the surface, which can be described as the reduction of the catalyst. The second step reaction involved the occupation of an oxygen vacancy from the bulk to the surface, which can be described as the re-oxidation of the catalyst [73,74]. In this work, toluene was oxidation once connected with the active oxygen species at oxygen vacancies, causing the consumption of lattice oxygen, meanwhile, the surface active oxygen species was replenished by the gas-phase oxygen, resulting in the regeneration of the lattice oxygen. Thus, it can be inferred that the oxidation of toluene over the Cu_1Ce_3 catalyst involves a Mars-van-Krevelen (MvK) mechanism.

4. Conclusion

A series of Cu-Ce binary oxides with different Ce/Cu molar ratios were synthesized via a facile co-precipitation approach. A majority of Cu ions were incorporated into CeO_2 to form the O_v-Cu^{2+}-O-Ce^{4+} connection, generating the structural defects and oxygen vacancies. This synergistic effect boosts the catalytic activity of Cu-Ce binary oxides. According to a battery of characterization results, it reveals Cu_1Ce_3 catalyst possess higher specific surface area, better low-temperature reducibility, and stronger Cu-Ce synergistic effect than other samples. Based on catalytic activity tests, it confirmed that the Cu_1Ce_3 catalyst exhibited better catalytic performance with 99.10% toluene removal efficiency and 97.28% CO_2 selectivity at 200 °C, which is consistent with the characterization results. Moreover, the Cu_1Ce_3 catalyst exhibited a certain activity under high GHSV and low O_2 concentration, also presented considerable durability and moisture resistance. Besides, the catalytic performance was slightly facilitated in the presence of NO and gaseous O_2 played an indispensable role in the regeneration of lattice oxygen. In-situ DRIFTs revealed the process of toluene catalyst oxidation over Cu_1Ce_3 catalyst. A large portion of toluene molecules could be connected with the interface lattice oxygen, after that, the catalytic process started from the abstraction of H atoms on the methyl group. The primary intermediate is considered to be benzyl alcohol, and the oxidation of benzyl alcohol into benzoic acid is identified as the rate-determining step. Meanwhile, a small number of toluene molecules could be oxidized into benzoic acid by chemisorbed oxygen species. In subsequent steps, the benzoic acid was oxidized successively into maleic anhydride, finally converted into CO_2 and H_2O. The consumed lattice oxygen was replenished by gaseous O_2 via the redox cycle $Ce^{3+} + Cu^{2+} \Leftrightarrow Ce^{4+} + Cu^{+}$. Thus, the catalytic oxidation process of toluene over the Cu_1Ce_3 catalyst conforms to the MvK mechanism.

CRediT authorship contribution statement

Binghong Song: Conceptualization, Methodology, Investigation, Writing – original draft, Data curation, Validation. **Caiting Li:** Conceptualization, Supervision, Writing - review & editing, Funding acquisition. **Xueyu Du:** Methodology, Writing - review & editing. **Shanhong Li:** Supervision. **Yindi Zhang:** Writing - review & editing. **Yue Lyu:** Writing - review & editing. **Qihao Zhou:** Writing - review & editing.

Declaration of competing interest

The authors declare that they have no known competing financial interests or personal relationships that could have appeared to influence the work reported in this paper.

Acknowledgments

This work was supported by the Key Research and Development Program of Hunan Province in China (2018SK2032).

Appendix A. Supplementary data

Supplementary data to this article can be found online at https://doi.org/10.1016/j.fuel.2021.121654.

References

[1] Wang H, Nie L, Li J, Wang Y, Wang G, Wang J, et al. Characterization and assessment of volatile organic compounds (VOCs) emissions from typical industries. Chin Sci Bull 2013;58:724–30.
[2] Zhang X, Gao B, Creamer AE, Cao C, Li Y. Adsorption of VOCs onto engineered carbon materials: A review. J Hazard Mater 2017;338:102–23.
[3] Hakim M, Broza YY, Barash O, Peled N, Phillips M, Amann A, et al. Volatile organic compounds of lung cancer and possible biochemical pathways. Chem Rev 2012;112:5949–66.
[4] Zheng C, Shen J, Zhang Y, Huang W, Zhu X, Wu X, et al. Quantitative assessment of industrial VOC emissions in China: Historical trend, spatial distribution, uncertainties, and projection. Atmos Environ 2017;150:116–25.
[5] Du X, Li C, Zhang J, Zhao L, Li S, Lyu Y, et al. Highly efficient simultaneous removal of HCHO and elemental mercury over Mn-Co oxides promoted Zr-AC samples. J Hazard Mater 2021;408:124830. https://doi.org/10.1016/j.jhazmat.2020.124830.
[6] Shu Y, Ji J, Xu Y, Deng J, Huang H, He M, et al. Promotional role of Mn doping on catalytic oxidation of VOCs over mesoporous TiO_2 under vacuum ultraviolet (VUV) irradiation. Appl Catal B 2018;220:78–87.
[7] Lee JE, Ok YS, Tsang DCW, Song J, Jung S-C, Park Y-K. Recent advances in volatile organic compounds abatement by catalysis and catalytic hybrid processes: A critical review. Sci Total Environ 2020;719:137405. https://doi.org/10.1016/j.scitotenv.2020.137405.
[8] Jakubek T, Hudy C, Indyka P, Nowicka E, Golunski S, Kotarba A. Effect of noble metal addition to alkali-exchanged cryptomelane on the simultaneous soot and VOC combustion activity. Catal Commun 2019;132:105807. https://doi.org/10.1016/j.catcom.2019.105807.
[9] Guo Y, Wen M, Li G, An T. Recent advances in VOC elimination by catalytic oxidation technology onto various nanoparticles catalysts: a critical review. Appl Catal B 2021;281:119447. https://doi.org/10.1016/j.apcatb.2020.119447.
[10] Peng R, Sun X, Li S, Chen L, Fu M, Wu J, et al. Shape effect of Pt/CeO 2 catalysts on the catalytic oxidation of toluene. Chem Eng J 2016;306:1234–46.
[11] Kim SC, Park Y-K, Nah JW. Property of a highly active bimetallic catalyst based on a supported manganese oxide for the complete oxidation of toluene. Powder Technol 2014;266:292–8.
[12] Du J, Qu Z, Dong C, Song L, Qin Y, Huang Na. Low-temperature abatement of toluene over Mn-Ce oxides catalysts synthesized by a modified hydrothermal approach. Appl Surf Sci 2018;433:1025–35.
[13] Kamal MS, Razzak SA, Hossain MM. Catalytic oxidation of volatile organic compounds (VOCs) – A review. Atmos Environ 2016;140:117–34.
[14] Tomatis M, Xu H-H, He J, Zhang X-D. Recent development of catalysts for removal of volatile organic compounds in flue gas by combustion: A review. J Chem 2016;2016:1–15.
[15] Heynderickx PM, Thybaut JW, Poelman H, Poelman D, Marin GB. The total oxidation of propane over supported Cu and Ce oxides: A comparison of single and binary metal oxides. J Catal 2010;272:109–20.
[16] Delimaris D, Ioannides T. VOC oxidation over CuO–CeO_2 catalysts prepared by a combustion method. Appl Catal B 2009;89:295–302.
[17] Zeng Y, Wang Y, Song F, Zhang S, Zhong Q. The effect of CuO loading on different method prepared CeO_2 catalyst for toluene oxidation. Sci Total Environ 2020;712:135635. https://doi.org/10.1016/j.scitotenv.2019.135635.
[18] Galvita VV, Filez M, Poelman H, Bliznuk V, Marin GB. The role of different types of CuO in CuO–CeO_2/Al_2O_3 for total oxidation. Catal Lett 2014;144(1):32–43. https://doi.org/10.1007/s10562-013-1144-x.
[19] Menon U, Galvita VV, Constales D, Alexopoulos K, Yablonsky G, Marin GB. Microkinetics for toluene total oxidation over CuO–CeO_2/Al_2O_3. Catal Today 2015;258:214–24. https://doi.org/10.1016/j.cattod.2015.07.015.
[20] Lu H, Kong X, Huang H, Zhou Y, Chen Y. Cu-Mn-Ce ternary mixed-oxide catalysts for catalytic combustion of toluene. J Environ Sci (China) 2015;32:102–7. https://doi.org/10.1016/j.jes.2014.11.015.
[21] Ismail A, Li M, Zahid M, Fan L, Zhang C, Li Z, et al. Effect of strong interaction between Co and Ce oxides in $Co_xCe_{1-x}O_{2-\delta}$ oxides on its catalytic oxidation of toluene, Molecular. Catalysis 2021;502:111356. https://doi.org/10.1016/j.mcat.2020.111356.
[22] Liu Z-G, Chai S-H, Binder A, Li Y-Y, Ji L-T, Dai S. Influence of calcination temperature on the structure and catalytic performance of CuO_x-CoO_y-CeO_2 ternary mixed oxide for CO oxidation. Appl Catal A 2013;451:282–8. https://doi.org/10.1016/j.apcata.2012.10.023.
[23] Herschend B, Baudin M, Hermansson K. Electronic structure of the CeO_2(110) surface oxygen vacancy. Surf Sci 2005;599(1-3):173–86. https://doi.org/10.1016/j.susc.2005.09.045.

[24] Wang Q, Yeung KL, Bañares MA. Ceria and its related materials for VOC catalytic combustion: A review. Catal Today 2020;356:141–54. https://doi.org/10.1016/j.cattod.2019.05.016.

[25] Sun H, Liu Z, Chen S, Quan X. The role of lattice oxygen on the activity and selectivity of the OMS-2 catalyst for the total oxidation of toluene. Chem Eng J 2015;270:58–65. https://doi.org/10.1016/j.cej.2015.02.017.

[26] Gamarra D, Hornés A, Koppány Zs, Schay Z, Munuera G, Soria J, et al. Catalytic processes during preferential oxidation of CO in H2-rich streams over catalysts based on copper–ceria. J Power Sources 2007;169(1):110–6. https://doi.org/10.1016/j.jpowsour.2007.01.048.

[27] Zhao H, Li H, Pan Z, Feng F, Gu Y, Du J, et al. Design of CeMnCu ternary mixed oxides as soot combustion catalysts based on optimized Ce/Mn and Mn/Cu ratios in binary mixed oxides. Appl Catal B 2020;268:118422. https://doi.org/10.1016/j.apcatb.2019.118422.

[28] Luo M, Ma J, Lu J, Song Y, Wang Y. High-surface area CuO–CeO$_2$ catalysts prepared by a surfactant-templated method for low-temperature CO oxidation. J Catal 2007;246(1):52–9. https://doi.org/10.1016/j.jcat.2006.11.021.

[29] Papavasiliou J, Avgouropoulos G, Ioannides T. In situ combustion synthesis of structured Cu-Ce-O and Cu-Mn-O catalysts for the production and purification of hydrogen. Appl Catal B 2006;66(3-4):168–74. https://doi.org/10.1016/j.apcatb.2006.03.011.

[30] Chang Z, Zhao N, Liu J, Li F, Evans DG, Duan X, et al. Cu–Ce–O mixed oxides from Ce-containing layered double hydroxide precursors: Controllable preparation and catalytic performance. J Solid State Chem 2011;184(12):3232–9. https://doi.org/10.1016/j.jssc.2011.09.035.

[31] Li L, Zhang C, Chen F, Xiang Y, Yan J, Chu W. Facile fabrication of hollow structured Cu-Ce binary oxides and their catalytic properties for toluene combustion. Catal Today 2021;376:239–46. https://doi.org/10.1016/j.cattod.2020.05.038.

[32] Martinezarias A, Gamarra D, Fernandezgarcia M, Wang X, Hanson J, Rodriguez J. Comparative study on redox properties of nanosized CeO$_2$ and CuO/CeO$_2$ under CO/O$_2$. J Catal 2006;240:1–7. https://doi.org/10.1016/j.jcat.2006.02.026.

[33] He C, Yu Y, Chen C, Yue L, Qiao N, Shen Q, et al. Facile preparation of 3D ordered mesoporous CuOx–CeO$_2$ with notably enhanced efficiency for the low temperature oxidation of heteroatom-containing volatile organic compounds. RSC Advances 2013;3:19639. https://doi.org/10.1039/c3ra42566e.

[34] Piumetti M, Bensaid S, Andana T, Russo N, Pirone R, Fino D. Cerium-copper oxides prepared by solution combustion synthesis for total oxidation reactions: From powder catalysts to structured reactors. Appl Catal B 2017;205:455–68. https://doi.org/10.1016/j.apcatb.2016.12.054.

[35] Zhou G, Lan H, Yang X, Du Q, Xie H, Fu M. Effects of the structure of Ce-Cu catalysts on the catalytic combustion of toluene in air. Ceram Int 2013;39:3677–83. https://doi.org/10.1016/j.ceramint.2012.10.199.

[36] He C, Yu Y, Yue L, Qiao N, Li J, Shen Q, et al. Low-temperature removal of toluene and propanal over highly active mesoporous CuCeOx catalysts synthesized via a simple self-precipitation protocol. Appl Catal B 2014;147:156–66. https://doi.org/10.1016/j.apcatb.2013.08.039.

[37] Sumrunronnasak S, Chanlek N, Pimpha N. Improved CeCuOx catalysts for toluene oxidation prepared by aqueous cationic surfactant precipitation method. Mater Chem Phys 2018;216:143–52. https://doi.org/10.1016/j.matchemphys.2018.05.006.

[38] Zeng S, Liu K, Zhang Lu, Qin B, Chen T, Yin Y, et al. Deactivation analyses of CeO$_2$/CuO catalysts in the preferential oxidation of carbon monoxide. J Power Sources 2014;261:46–54. https://doi.org/10.1016/j.jpowsour.2014.03.043.

[39] Wu Z, Li M, Howe J, Meyer HM, Overbury SH. Probing defect sites on CeO$_2$ nanocrystals with well-defined surface planes by Raman spectroscopy and O$_2$ adsorption. Langmuir 2010;26(21):16595–606. https://doi.org/10.1021/la101723w.

[40] Dai Q, Huang H, Zhu Yu, Deng W, Bai S, Wang X, et al. Catalysis oxidation of 1,2-dichloroethane and ethyl acetate over ceria nanocrystals with well-defined crystal planes. Appl Catal B 2012;117-118:360–8. https://doi.org/10.1016/j.apcatb.2012.02.001.

[41] Ilieva L, Pantaleo G, Ivanov I, Venezia AM, Andreeva D. Gold catalysts supported on CeO$_2$ and CeO$_2$–Al$_2$O$_3$ for NO$_x$ reduction by CO. Appl Catal B 2006;65(1-2):101–9. https://doi.org/10.1016/j.apcatb.2005.12.014.

[42] Spanier JE, Robinson RD, Zhang F, Chan S-W, Herman IP, Size-dependent properties ofCeO2−ynanoparticles as studied by Raman scattering, Phys Rev B, 64 (2001).https://doi.org/10.1103/PhysRevB.64.245407.

[43] Li X, Xin X, Peng Z, Zhang H, Yi C, Li B. Analysis of the spatial variability of land surface variables for ET estimation: case study in HiWATER campaign. Remote Sensing 2018;10(2):91. https://doi.org/10.3390/rs10010091.

[44] Gurbani A, Ayastuy JL, González-Marcos MP, Gutiérrez-Ortiz MA. CuO–CeO$_2$ catalysts synthesized by various methods: comparative study of redox properties. Int J Hydrogen Energy 2010;35(20):11582–90. https://doi.org/10.1016/j.ijhydene.2010.04.045.

[45] Hernández WY, Centeno MA, Ivanova S, Eloy P, Gaigneaux EM, Odriozola JA. Cu-modified cryptomelane oxide as active catalyst for CO oxidation reactions. Appl Catal B 2012;123-124:27–35. https://doi.org/10.1016/j.apcatb.2012.04.024.

[46] Kim SC, Shim WG. Catalytic combustion of VOCs over a series of manganese oxide catalysts. Appl Catal B 2010;98(3-4):180–5.

[47] Liao Y, Zhang X, Peng R, Zhao M, Ye D. Catalytic properties of manganese oxide polyhedra with hollow and solid morphologies in toluene removal. Appl Surf Sci 2017;405:20–8. https://doi.org/10.1016/j.apsusc.2017.02.012.

[48] Yu D, Liu Y, Wu Z. Low-temperature catalytic oxidation of toluene over mesoporous MnO–CeO$_2$/TiO$_2$ prepared by sol–gel method. Catal Commun 2010;11(8):788–91.

[49] Huang H, Hu P, Huang H, Chen J, Ye X, Leung DYC. Highly dispersed and active supported Pt nanoparticles for gaseous formaldehyde oxidation: Influence of particle size. Chem Eng J 2014;252:320–6. https://doi.org/10.1016/j.cej.2014.04.108.

[50] Sheng J, Li C, Zhao L, Du X, Gao L, Zeng G. Efficient removal of HCHO from simulated coal combustion flue gas using CuO-CeO$_2$ supported on cylindrical activated coke. Fuel 2017;197:397–406. https://doi.org/10.1016/j.fuel.2017.02.056.

[51] Aranda A, Agouram S, López JM, Mastral AM, Sellick DR, Solsona B, et al. Oxygen defects: The key parameter controlling the activity and selectivity of mesoporous copper-doped ceria for the total oxidation of naphthalene. Appl Catal B 2012;127:77–88. https://doi.org/10.1016/j.apcatb.2012.07.033.

[52] Avgouropoulos G, Ioannides T. Effect of synthesis parameters on catalytic properties of CuO-CeO$_2$. Appl Catal B 2006;67:1–11. https://doi.org/10.1016/j.apcatb.2006.04.005.

[53] Tsoncheva T, Issa G, Blasco T, Dimitrov M, Popova M, Hernández S, et al. Catalytic VOCs elimination over copper and cerium oxide modified mesoporous SBA-15 silica. Appl Catal A 2013;453:1–12. https://doi.org/10.1016/j.apcata.2012.12.007.

[54] Zeng Y, Haw K-G, Wang Z, Wang Y, Zhang S, Hongmanorom P, et al. Double redox process to synthesize CuO-Ce$_{O2}$ catalysts with strong Cu-Ce interaction for efficient toluene oxidation. J Hazard Mater 2021;404:124088. https://doi.org/10.1016/j.jhazmat.2020.124088.

[55] Chen C-C, Lin L, Ye R-P, Huang L, Zhu L-B, Huang Y-Y, et al. Construction of Cu-Ce composite oxides by simultaneous ammonia evaporation method to enhance catalytic performance of Ce-Cu/SiO$_2$ catalysts for dimethyl oxalate hydrogenation. Fuel 2021;290:120083. https://doi.org/10.1016/j.fuel.2020.120083.

[56] Khemthong P, Photai P, Grisdanurak N. Structural properties of CuO/TiO$_2$ nanorod in relation to their catalytic activity for simultaneous hydrogen production under solar light. Int J Hydrogen Energy 2013;38(36):15992–6001. https://doi.org/10.1016/j.ijhydene.2013.10.065.

[57] He C, Xu B-T, Shi J-W, Qiao N-L, Hao Z-P, Zhao J-L. Catalytic destruction of chlorobenzene over mesoporous ACeOx (A=Co, Cu, Fe, Mn, or Zr) composites prepared by inorganic metal precursor spontaneous precipitation. Fuel Process Technol 2015;130:179–87. https://doi.org/10.1016/j.fuproc.2014.10.008.

[58] Liu M, Li C, Zeng Q, Du X, Gao L, Li S, et al. Study on removal of elemental mercury over MoO$_3$-CeO$_2$/cylindrical activated coke in the presence of SO$_2$ by Hg-temperature-programmed desorption. Chem Eng J 2019;371:666–78. https://doi.org/10.1016/j.cej.2019.04.088.

[59] Du X, Li C, Zhao L, Zhang J, Gao L, Sheng J, et al. Promotional removal of HCHO from simulated flue gas over Mn-Fe oxides modified activated coke. Appl Catal B 2018;232:37–48. https://doi.org/10.1016/j.apcatb.2018.03.034.

[60] Gao L, Li C, Lu P, Zhang J, Du X, Li S, et al. Simultaneous removal of Hg0 and NO from simulated flue gas over columnar activated coke granules loaded with La$_2$O$_3$-CeO$_2$ at low temperature. Fuel 2018;215:30–9. https://doi.org/10.1016/j.fuel.2017.11.008.

[61] Li WB, Wang JX, Gong H. Catalytic combustion of VOCs on non-noble metal catalysts. Catal Today 2009;148:81–7. https://doi.org/10.1016/j.cattod.2009.03.007.

[62] Wang Y, Zhang F, Cui W, Chen K, Zhao R, Zhang Z. The FvPHR1 transcription factor control phosphate homeostasis by transcriptionally regulating miR399a in woodland strawberry. Plant Sci 2019;280:258–68. https://doi.org/10.1016/j.plantsci.2018.12.025.

[63] Chen B-B, Shi C, Crocker M, Wang Yu, Zhu A-M. Catalytic removal of formaldehyde at room temperature over supported gold catalysts. Appl Catal B 2013;132-133:245–55. https://doi.org/10.1016/j.apcatb.2012.11.028.

[64] Yang W, Su Z, Xu Z, Yang W, Peng Y, Li J. Comparative study of α-, β-, γ- and δ-MnO$_2$ on toluene oxidation: Oxygen vacancies and reaction intermediates. Appl Catal B 2020;260:118150. https://doi.org/10.1016/j.apcatb.2019.118150.

[65] Mirji SA, Halligudi SB, Sawant DP, Patil KR, Gaikwad AB, Pradhan SD. Adsorption of toluene on Si(100)/SiO$_2$ substrate and mesoporous SBA-15. Colloids Surf, A 2006;272:220–6. https://doi.org/10.1016/j.colsurfa.2005.07.019.

[66] Dong C, Qu Z, Qin Y, Fu Q, Sun H, Duan X. Revealing the highly catalytic performance of spinel CoMn$_2$O$_4$ for toluene oxidation: involvement and replenishment of oxygen species using in situ designed-TP techniques. ACS Catal 2019;9:6698–710. https://doi.org/10.1021/acscatal.9b01324.

[67] Lyu Y, Li C, Du X, Zhu Y, Zhang Y, Li S. Catalytic oxidation of toluene over MnO$_2$ catalysts with different Mn (II) precursors and the study of reaction pathway. Fuel 2020;262:116610. https://doi.org/10.1016/j.fuel.2019.116610.

[68] Yang X, Yu X, Jing M, Song W, Liu J, Ge M. Defective Mn $_x$Zr$_{1- x}$O$_2$ solid solution for the catalytic oxidation of toluene: insights into the oxygen vacancy contribution. ACS Appl Mater Interfaces 2019;11:730–9. https://doi.org/10.1021/acsami.8b17062.

[69] Zhao C, Hao Q, Zhang Q, Yan N, Liu J, Dou B, et al. Catalytic self-sustained combustion of toluene and reaction pathway over Cu$_x$Mn$_{1-x}$Ce$_{0.75}$Zr$_{0.25}$/TiO$_2$ catalysts. Appl Catal A 2019;569:66–74. https://doi.org/10.1016/j.apcata.2018.10.034.

[70] Liu B, Zhan Y, Xie R, Huang H, Li K, Zeng Y, et al. Efficient photocatalytic oxidation of gaseous toluene in a bubbling reactor of water. Chemosphere 2019;233:754–61. https://doi.org/10.1016/j.chemosphere.2019.06.002.

[71] Santos VP, Pereira MFR, Órfão JJM, Figueiredo JL. The role of lattice oxygen on the activity of manganese oxides towards the oxidation of volatile organic compounds. Appl Catal B 2010;99:353–63. https://doi.org/10.1016/j.apcatb.2010.07.007.

[72] Shi F, Wang F, Dai H, Dai J, Deng J, Liu Y, et al. and dumbbell-like MnO_2: Highly active catalysts for the combustion of toluene. Appl Catal A 2012;433-434:206–13. https://doi.org/10.1016/j.apcata.2012.05.016.

[73] Burgos N. Deep oxidation of VOC mixtures with platinum supported on Al_2O_3/Al monoliths. Appl Catal B 2002;38:251–8.

[74] Radic N, Grbic B, Terlecki-Baricevic A. Kinetics of deep oxidation of n-hexane and toluene over Pt/Al_2O_3 catalysts. Appl Catal B 2004;50:153–9. https://doi.org/10.1016/j.apcatb.2004.01.011.